3D Characterization for Your 3D Material Structures.

- See even smaller sub-micron details
- Unprecedented image clarity at unprecedented speed enabled by AI
- UX designed for novices and experts alike

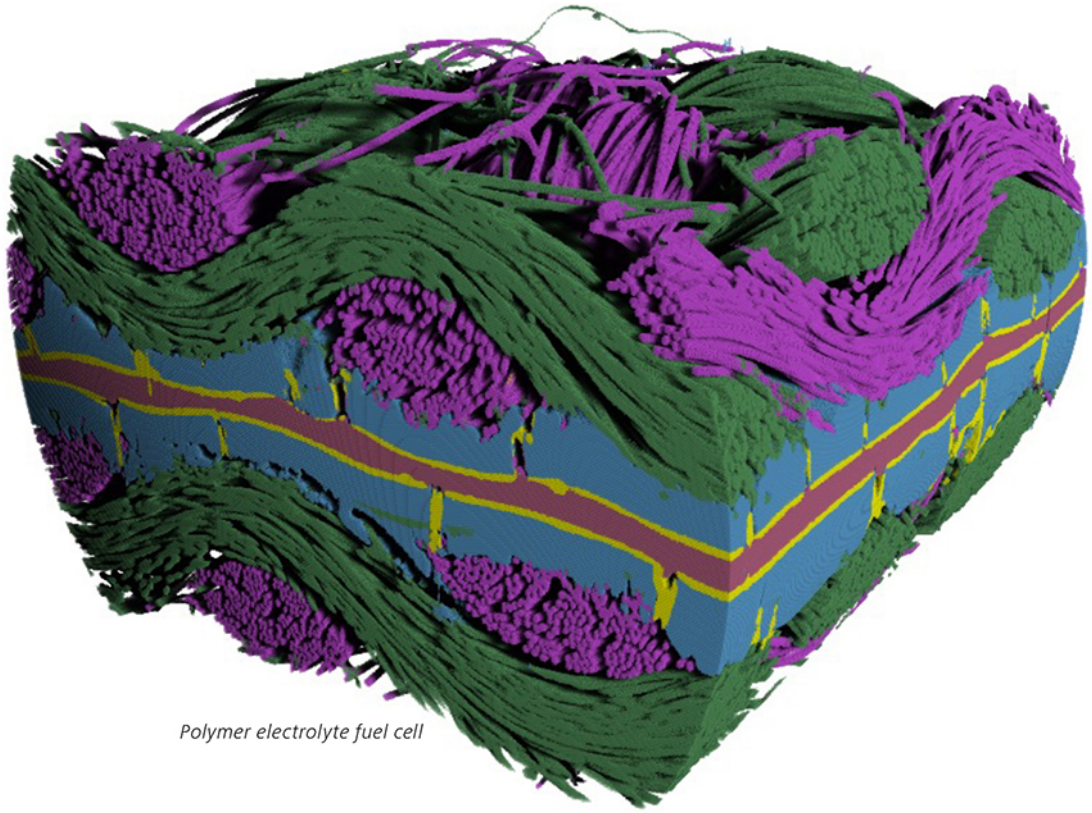

Polymer electrolyte fuel cell

Introducing ZEISS Xradia 630 Versa 3D X-ray Microscope

Seeing inside advanced materials can provide critical clues related to how structure affects performance. Achieving this insight at the microscale requires the clearest and highest-resolution 3D X-ray images. Use the newest ZEISS Xradia Versa 3D X-ray microscope (XRM) for nondestructive characterization of the finest sub-micron features within your materials. Leverage deep learning for the clearest 3D images across large representative volumes. Enjoy an intuitive, guided user experience that makes XRM technology accessible to all user skill levels.

ZEISS

Seeing beyond

ADVANCED MATERIALS
www.advmat.de

Tough Hydrogel Electrolytes for Anti-Freezing Zinc-Ion Batteries

*Yichen Yan, Sidi Duan, Bo Liu, Shuwang Wu, Yousif Alsaid, Bowen Yao, Sunny Nandi, Yingjie Du, Ta-Wei Wang, Yuzhang Li, and Ximin He**

As the soaring demand for energy storage continues to grow, batteries that can cope with extreme conditions are highly desired. Yet, existing battery materials are limited by weak mechanical properties and freeze-vulnerability, prohibiting safe energy storage in devices that are exposed to low temperature and unusual mechanical impacts. Herein, a fabrication method harnessing the synergistic effect of co-nonsolvency and "salting-out" that can produce poly(vinyl alcohol) hydrogel electrolytes with unique open-cell porous structures, composed of strongly aggregated polymer chains, and containing disrupted hydrogen bonds among free water molecules, is introduced. The hydrogel electrolyte simultaneously combines high strength (tensile strength 15.6 MPa), freeze-tolerance (< −77 °C), high mass transport (10× lower overpotential), and dendrite and parasitic reactions suppression for stable performance (30 000 cycles). The high generality of this method is further demonstrated with poly(*N*-isopropylacrylamide) and poly(*N*-tertbutylacrylamide-*co*-acrylamide) hydrogels. This work takes a further step toward flexible battery development for harsh environments.

1. Introduction

As the soaring demand and emerging application scenarios for energy storage continue, batteries that can operate in extreme conditions are a critical need, especially for soft electrical devices. Safe and stable operation of robust batteries to power fast-advancing systems such as wearable devices[1,2] and soft robotics[3–8] plays a pivotal role in revolutionizing healthcare, energy,[9] environments, and machine autonomy and intelligence.[3] Mechanically, wearable electronic devices and soft robots experience various mechanical impacts or complex deformations such as hitting, tearing, and puncturing. Thermally, they need to endure 0 °C to −20 °C for some space exploration[10] and down to −40 °C or ideally −61 °C in high latitude or altitude areas.[11] Therefore, the batteries as their power supply components are also required to be not only soft and flexible[9] but also impact-resistant[12] and anti-freezing. To achieve this goal, it is crucial to develop novel soft electrolyte materials (including separators) capable of maintaining high ionic conductivity and withstanding the impacts to prevent shorting and resist dendrite growth for battery stability[13–16] under a broad range of temperatures.

While lithium batteries with organic electrolytes face challenges such as depleting limited-reserve-elements (e.g., cobalt), toxicity, high reactivity, and flammability, and solid electrolytes fall short in conductivity, aqueous zinc batteries have attracted tremendous interest in recent years due to their intrinsic safety, eco-friendliness, and low production cost.[17–24] Within aqueous systems, quasi-solid hydrogel electrolytes outperform liquid electrolytes as they can be leakage-free, suppress dendrite growth, and inhibit hazardous side reactions,[25–33] while maintaining high flexibility. Anti-freezing hydrogel electrolytes were successfully developed by adding organic solvents or concentrated salts, polymer modification, and so on.[34–50] However, a hydrogel electrolyte that is mechanically robust, thermally stable, and mass transport friendly at the same time is yet to be developed, owing to the following obstacles. First, previously reported anti-freezing strategies by salts or additives will harm the mechanical strength. For example, the addition of calcium chloride,[51] lithium chloride,[52] zinc perchlorate, zinc nitrate, zinc triflate, zinc iodide,[34] or ethylene glycol[47] suppresses the freezing temperature but unfortunately deteriorates the ultimate tensile strength,[34,47,51,52] fracture toughness,[51] toughness,[47,52] and elongation at break[47,52] of the hydrogel due to the "salting-in" effect which decreases the polymer aggregation.[53] As a result, most of the reported anti-freezing hydrogel electrolytes are mechanically weak (see Table S1,

Y. Yan, S. Duan, S. Wu, Y. Alsaid, B. Yao, Y. Du, T.-W. Wang, X. He
Department of Materials Science and Engineering
University of California, Los Angeles
Los Angeles, CA 90095, USA
E-mail: ximinhe@ucla.edu
B. Liu, S. Nandi, Y. Li
Department of Chemical and Biomolecular Engineering
University of California, Los Angeles
Los Angeles, CA 90095, USA
S. Nandi
Department of Physics
Tezpur University
Assam 784028, India
X. He
California Nanosystems Institute
Los Angeles, CA 90095, USA
The ORCID identification number(s) for the author(s) of this article can be found under https://doi.org/10.1002/adma.202211673.

DOI: 10.1002/adma.202211673

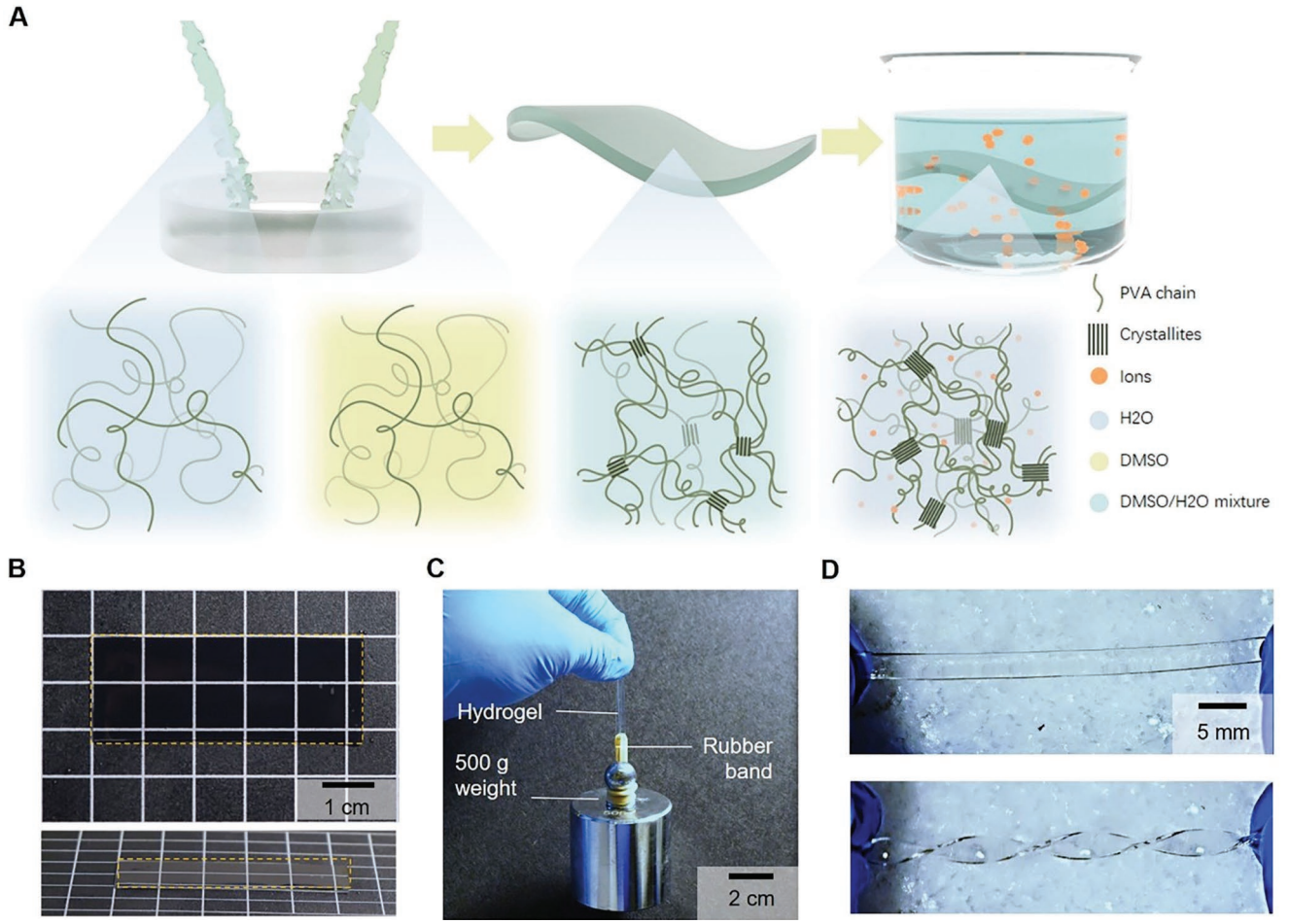

Figure 1. Strong and anti-freezing hydrogel electrolyte through the synergy of co-nonsolvency and "salting-out". A) Schematics of the fabrication. The PVA/water and PVA/DMSO solutions were mixed to induce co-nonsolvency to form a gel, which was then soaked in a salt solution to go through "salting-out". B) Photographs of the hydrogel electrolyte. Top: Top view. Bottom: Side view. The transparent hydrogel is outlined with yellow dashed lines for visibility. C) A photograph displaying a hydrogel strip lifting a 500 g weight, showing its strength. D) Photographs of twisting a hydrogel strip at −30 °C, showing its anti-freezing ability.

Supporting Information) and cannot match the strength of the commercial separator Celgard[54] and National Aeronautics and Space Administration (NASA) standards.[55] Second, strength and mass transport are typically inversely correlated;[56,57] strong polymers generally possess high crystallinity and solid content, while ionic conduction is favored in the amorphous or porous structure, which compromises strength. Third, organic additives sacrifice the intrinsic safety advantage of the aqueous system[58] and inhibit salt ion solvation, leading to precipitations that compromise the low-temperature performance.[18]

Here, we synergistically employ the co-nonsolvency effect from the polymer's mixed solvents and the "salting-out" effect from an anti-freezing salt solution (**Figure 1**A,B) to produce mechanically robust (Figure 1C), anti-freezing (Figure 1D), high-mass-transport, and organic solvent-free hydrogel electrolytes. "Salting-out" ions, such as potassium ion (K^+) and acetate, are effective in toughening hydrogels via ion-promoted chain aggregation while maintaining the high water content.[34,53,59,60] Co-nonsolvency[61,62] also influences the chain aggregation, where adding cosolvent to the precursor promotes the formation of open-cell porous structures with densified polymer network; thus, enhancing both mass transport (10× lower overpotential compared to the less porous counterparts, **Figure 2**F) and strength (Figure 2B,C). The "salting-out" is achieved by an exemplary salt mixture: potassium acetate (KAc), which combines "salting-out" and anti-freezing abilities, mixed with zinc acetate ($ZnAc_2$), a compatible zinc ion (Zn^{2+})-containing salt. Poly(vinyl alcohol) (PVA) is chosen as the exemplary polymer because it exhibits both "salting-out"[59] and co-nonsolvency effects.[61] Benefitting from both effects, such a hydrogel, as a wet material containing mostly liquid, is even stronger than dry wristbands materials[63] (15.6 MPa vs 11.6 MPa). The hydrogel electrolyte is compatible with the polyaniline cathode (composed only of abundant elements) and can be made into highly stable batteries at low temperatures (>30 000 cycles at −20 °C, negligible decrease in capacity). This presents its potential to be used in soft devices, which demand mechanical and electrochemical durability in harsh environments.

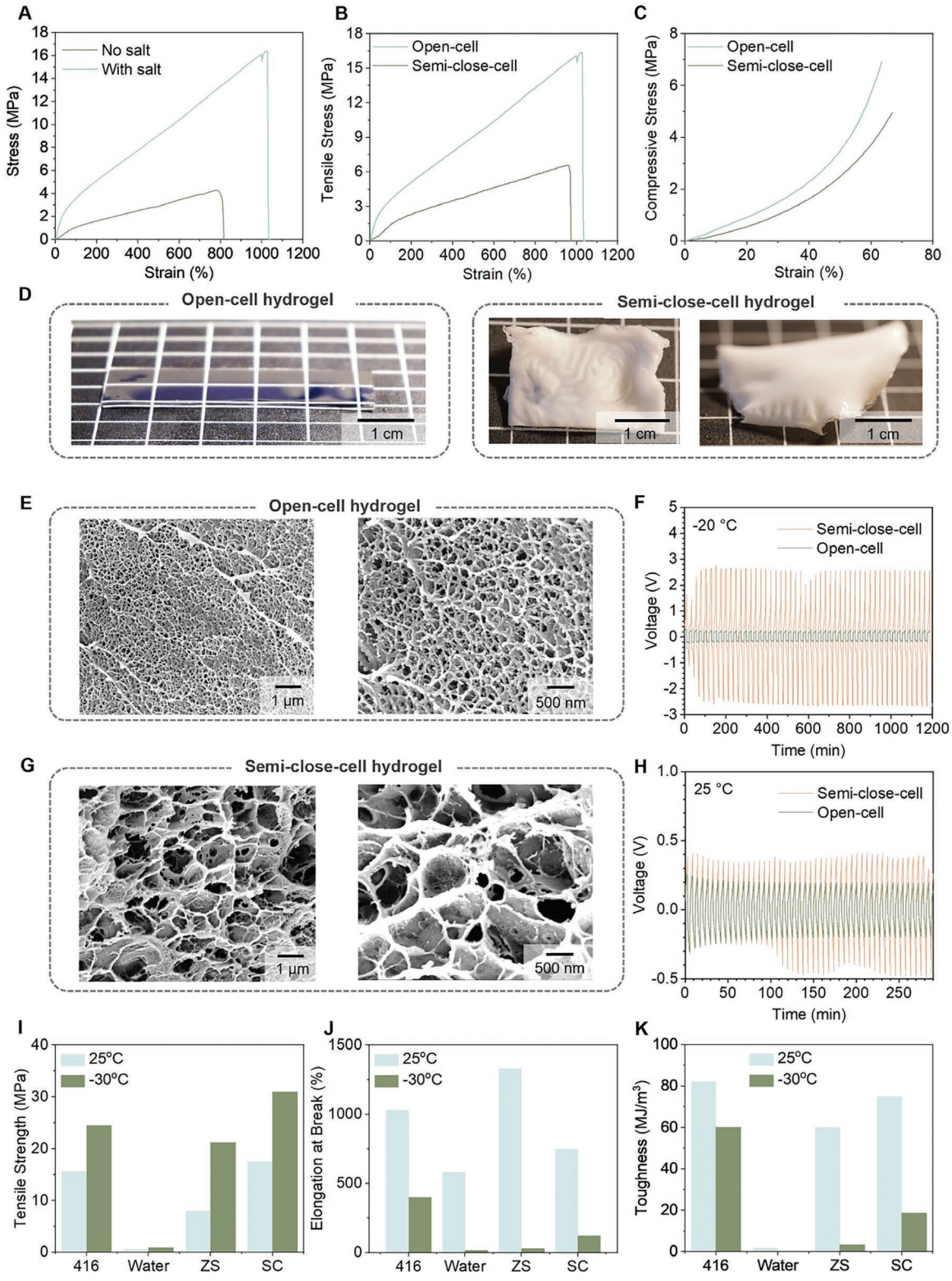

Figure 2. Synergistic effect of "salting-out" and co-nonsolvency. A) Stress–strain curve of the co-nonsolvency-"salting-out" hydrogel and the co-nonsolvency-only hydrogel. B) Tensile and C) compression tests of the co-nonsolvency-"salting-out" hydrogel and the "salting-out"-only hydrogel. D) Photographs of the open-cell hydrogels (from co-nonsolvency) showing the smooth and flat surfaces, and semi-closed-cell hydrogels (no co-nonsolvency) showing the wrinkled and curved surfaces. E,G) SEM images of the open-cell and semi-closed-cell hydrogels, respectively. F,H) Voltage profiles of Zn||Zn symmetric cell made with open-cell and semi-closed-cell hydrogel electrolytes at –20 °C and 25 °C, respectively. I–K) Tensile test results of the hydrogels with different solutions at 25 °C and –30 °C, where ZS = zinc sulfate and SC = sodium citrate.

2. Results and Discussion

2.1. Optimizing the "Dual-Salt" Solution

A Zn^{2+}-containing salt solution that exhibits both "salting-out" and anti-freezing abilities is needed to achieve the desired electrolyte properties. While a single salt that satisfies all three criteria does not exist to the best of our knowledge (Table S2 and Figures S1A and S2, Supporting Information), a salt mixture can be used, in which the first salt is "salting-out" and anti-freezing and the second salt contains Zn^{2+} ions and can form a homogeneous mixture with the first salt. An example of such a mixture is composed of KAc and $ZnAc_2$. KAc is one of the few salts that exhibit the combination of "salting-out" and anti-freezing; by contrast, calcium chloride and zinc perchlorate exhibit anti-freezing yet "salting-in" which weakens the hydrogel, while zinc sulfate, sodium sulfate, sodium carbonate, and sodium citrate exhibit "salting-out" yet weak anti-freezing abilities. While sodium acetate and potassium citrate exhibit both abilities, their anti-freezing abilities are experimentally measured to be inferior to that of KAc (Figure S1B, Supporting Information). In addition, potassium acetate can better strengthen the PVA compared to sodium acetate because K^+ has a stronger "salting-out" effect than sodium ions.[53] These justify the choice of KAc. As for $ZnAc_2$, it can introduce Zn^{2+} ions without introducing an anion that forms precipitates with K^+ at high concentrations (e.g., sulfate, Figure S3, Supporting Information). Overall, KAc/$ZnAc_2$ is selected because such a mixture yields a Zn^{2+}-containing solution with strong "salting-out" and anti-freezing properties. Acetate ions contained in both salts can suppress the parasitic reactions on the Zn anodes, as an additional benefit.[64]

KAc/$ZnAc_2$ solution can be made into ultrahigh concentration benefitting from the high solubility limit of KAc (≈75 wt%, Figure S4, Supporting Information) and the fact that KAc can increase the solubility of $ZnAc_2$. While a high concentration benefits the anti-freezing and "salting-out" ability of the solution, it could impede ion mobility and cause high overpotential or polarization during battery operation. A series of solutions were used as examples to demonstrate the influence of the salt concentrations on the solution properties, which were named according to the mass ratio of KAc/$ZnAc_2 \cdot 2H_2O/H_2O$ (named 317, 416, 515, 614, and 713 solutions, respectively. See also Table S3, Supporting Information). Their solid–liquid transition temperatures were measured by differential scanning calorimetry (DSC, Figure S5, Supporting Information), which was below −20 °C for all and decreased with increasing KAc concentration, reaching −39 °C for the 416 solution and < −85 °C for the 515 solution. The anti-freezing ability originated from the disrupted hydrogen bonding which is evident in the Raman spectroscopy results (Figure S6 and Table S4, Supporting Information), in which the relative quantity of the strongly hydrogen-bonded water (3230 cm^{-1}) and the moderately hydrogen-bonded water (3420 cm^{-1}) were altered with the addition of the salts.[65]

Aqueous KAc/$ZnAc_2$ solutions have been reported as stability-window-improving electrolytes[66,67] while their anti-freezing ability remains elusive. To demonstrate this, Zn‖Cu half cells with KAc/$ZnAc_2$ electrolytes were tested at 25 °C, −20 °C, −30 °C, and −40 °C (Figures S7 and S8, Supporting Information). When lower KAc concentrations were used, the appearance of polarization shifted to lower temperatures and higher current densities. For example, the 515 solution (45 wt% KAc)-containing cell did not show polarization until the current density reached 0.8 mA cm^{-2} at −20 °C, while the 614 solution (55 wt% KAc)-containing cell already showed polarization at 0.4 mA cm^{-2} current density. In summary, high salt concentration favors anti-freezing ability and mechanical strength, while relatively low concentration benefits battery performance. Based on these results, the 416 solution was chosen for its excellent anti-freezing ability (−39 °C), while also supporting decent current densities with reasonable overpotential at low temperatures without the appearance of polarization: 1 mA cm^{-2}, 150 mV, at −20 °C (Figure S7E, Supporting Information), or 0.6 mA cm^{-2}, 200 mV, at −30 °C (Figure S7F, Supporting Information). It is noteworthy that such a recipe for optimization is not exhaustive and other recipes could be developed based on different needs for the electrolyte.

2.2. Optimizing the Co-Nonsolvency Effect on PVA

Co-nonsolvency[61,68,69] has been recently found as an effective approach to generate porous structures with highly densified pore walls and interconnected pores for improving diffusion without compromising mechanical properties,[68] which benefits battery performance. This contrasts with conventional methods where increased porosity weakens the materials. Two physical descriptions exist for co-nonsolvency: "solvent complexation," whereby the two solvents prefer each other over the polymer chains, resulting in a solvent complex as a weak solvent for the polymer; and thus, chain aggregation[70] and "preferential adsorption," whereby one solvent prefers the polymer chains much more strongly than the other does, resulting in the weak solvent exclusion from the polymer matrix; and thus, polymer chain aggregation.[71–73] The mechanisms indicate that variables such as chain length, solvent ratio, aging time, and polymer concentration influence the co-nonsolvency effect, as observed in our systematic studies.

Variable tuning was conducted to produce an optimum hydrogel that meets the high demand in real-world applications. First, hydrogels were fabricated with a fixed PVA concentration (10 wt%) and varying dimethyl sulfoxide (DMSO)-to-water mass ratios (3:7–8:2) and molecular weights (M_w = 31–50k, 89–98k, and ≈195k, degree of hydrolysis > 98% for all). Results showed that higher M_w PVAs (longer PVA chains) yield stronger gels (Table S5 and Figure S9, Supporting Information), consistent with the Lake–Thomas theory.[74] In addition, longer chains will lead to more entanglements[75,76] which also enhance the strength. Comparison among hydrogels with the same M_w showed that the 6:4 ratio yielded the strongest gels, confirming previous reports.[61,77,78]

Then, the aging effect was studied (Table S6 and Figure S10, Supporting Information) with PVAs fabricated with a fixed concentration (10 wt%) and solvent ratio (6:4) and with varying molecular weights and aging times. Syneresis occurred during the aging process and the modulus, tensile strength, and toughness increased with increasing aging time for all samples with the same molecular weight. The increased aging

time allows more polymer chains to undergo conformation and spatial rearrangement, which leads to crystallite growth that strengthens the hydrogel.[79]

The strength can be further improved by utilizing PVA solutions of higher concentrations (Figure S11, Supporting Information). 15 wt% M_w = 195k PVA solutions were employed because higher concentrations would result in highly viscous solutions which are difficult to process. Similar to the 10 wt% PVA, the 15 wt% PVA also became stronger with aging (Table S7 and Figure S12, Supporting Information), demonstrating the generality of aging. In summary, a 6:4 ratio, higher M_w, higher polymer concentration, and longer aging time produce stronger hydrogel.

2.3. The Synergy of "Salting-Out" and Co-Nonsolvency

The synergistic effect of "salting-out" and co-nonsolvency produces better electrolytes than either of them alone, as we found in the hydrogels formed by co-nonsolvency (with water/DMSO mixed solvent) followed by "salting-out" through soaking in salt solutions. When comparing such a co-nonsolvency-"salting-out" hydrogel with the co-nonsolvency-only hydrogel (Figure 2A; Table S8-3 to S8-5, Supporting Information), the former showed much improved mechanical robustness (6 × modulus, 4 × tensile strength), demonstrating that "salting-out" treatment can effectively further enhance the strength of the co-nonsolvency-only hydrogel, possibly via the further growth of the crystalline domains generated from co-nonsolvency. Furthermore, "salting-out" also endowed the hydrogel with ions that are required for electrolytes.

When comparing the co-nonsolvency-"salting-out" hydrogel with the "salting-out"-only hydrogel formed by the regular freeze–thaw process, the former showed improved strength in both tensile and compression tests (Figure 2B,C; Table S8-1,8-5, Supporting Information), demonstrating the strengthening effect of the co-nonsolvency treatment. More importantly, the co-nonsolvency hydrogel had a "diffusion friendly" open-cell porous structure (Figure 2E; Figure S13C,D, Supporting Information), allowing for a homogeneous "salting-out" process to produce a hydrogel with a uniform structure and a smooth surface (Figure 2D). By contrast, PVA formed by the regular freeze–thaw process had a semi-closed-cell structure (Figure 2G; Figure S13A,B, Supporting Information) that hindered diffusion. "Salting-out" these PVA led to a wrinkled or curled surface (Figure 2D), which was possibly caused by the local strains generated from the inhomogeneous "salting-out" effect due to the slow diffusion of the ions. The non-smooth surface along with the diffusion-hindering microstructure renders such hydrogels not suitable for battery electrolytes because of the high overpotential and large voltage polarization.[61] By contrast, the co-nonsolvency-"salting-out" hydrogel showed 10× smaller overpotential in the Zn‖Zn cell test (0.23 V vs 2.5 V at −20 °C with 0.5 mA cm^{-2} current and 0.1 mA h cm^{-2} capacity, Figure 2F,H), originating from the open-cell structure. Furthermore, the small pores (≈100 nm) are believed to frustrate the growth of micrometer-sized dendrites.[80]

Apart from the superb mechanical and transport properties, PVA-416 also exhibits anti-freezing performance benefitting from the salt selection. To demonstrate this, hydrogels infiltrated with various types of liquids (zinc sulfate, sodium citrate,[59] 416 solution, and water) were stretched at 25 °C and −30 °C (Figure 2I–K). While similar strength can be achieved by other salts at 25 °C through "salting-out," at −30 °C, only the 416 solution-containing PVA can be considered as "stretchable" rather than "brittle", which benefits from the anti-freezing capability of the salt solution. In summary, the synergistic effect of co-nonsolvency and "salting-out" using the anti-freezing salt solutions provides a viable route to simultaneously enhance the strength, mass transport, and low-temperature tolerance of the hydrogel electrolytes.

2.4. Hydrogel Characterizations and Battery Performances

The co-nonsolvency-"salting-out" hydrogel (Table S8-5, Supporting Information, named PVA-416) was used for further characterization because it showed excellent mechanical, thermal, and mass transport properties and was organic solvent-free (Figure S14, Supporting Information). PVA-416 showed adequate transference number (0.517, Figure S15, Supporting Information) and ionic conductivity (49.8 mS cm at 25 °C, Figure S16, Supporting Information) to be used as a battery electrolyte. While the freezing temperature was inconclusive from the DSC measurement (Figure S17, Supporting Information) which possibly resulted from the complex water-ion-polymer interactions, the hydrogel still remained mechanically flexible after being held at −77 °C for 24 h (Figure S18, Supporting Information), demonstrating its excellent anti-freezing property. Mechanically, PVA-416 even showed much higher strength and toughness than the wetted glass fiber separators commonly used in zinc-ion batteries, in all the tensile (Figure S19A, Supporting Information), compression (Figure S19B, Supporting Information), and puncture force tests (Figures S19C and S20, Supporting Information, using a testing setup designed according to this literature[55]), demonstrating superior mechanical robustness. The outstanding 15.6 MPa tensile strength of the hydrogel (wet material) was even higher than that of the wearable electronics wristbands (dry solid material, 11.6 MPa on average).[63] In the calendar aging tests, the PVA-416-containing cell showed higher efficiency than the cell with the glass fiber separators (Figure S21, Supporting Information). The high strength of the hydrogel may retard dendritic growth, which effectively prevents the formation of dead Zn and improves efficiency.

The 100 µm thick PVA-416s were used to make coin cell batteries (Figure S22, Supporting Information) to test their electrochemical performances at various temperatures (25 °C, −20 °C, −30 °C, −40 °C, and −45 °C) with Zn foil anodes and polyaniline (PANi),[81–83] a cathode without using the endangered elements. Cyclic voltammetry (CV, Figure S23, Supporting Information) displayed the reversible peaks at 1.3 and 1.05 V versus Zn/Zn^{2+}, corresponding to the ion storage in the positively or negatively charged nitrogen sites in the oxidized or reduced PANi, respectively.[84] The rate performances (**Figure 3**A–C) at 0.1, 0.2, 0.5, 1, and 5 A g^{-1} were determined to be 96, 88, 76, 68, and 46 mA h g^{-1}, respectively at 25 °C, and 89, 82, 71, 59, and 18 mA h g^{-1}, respectively at −20 °C. When the temperature further dropped to −30 °C, capacities were determined to be

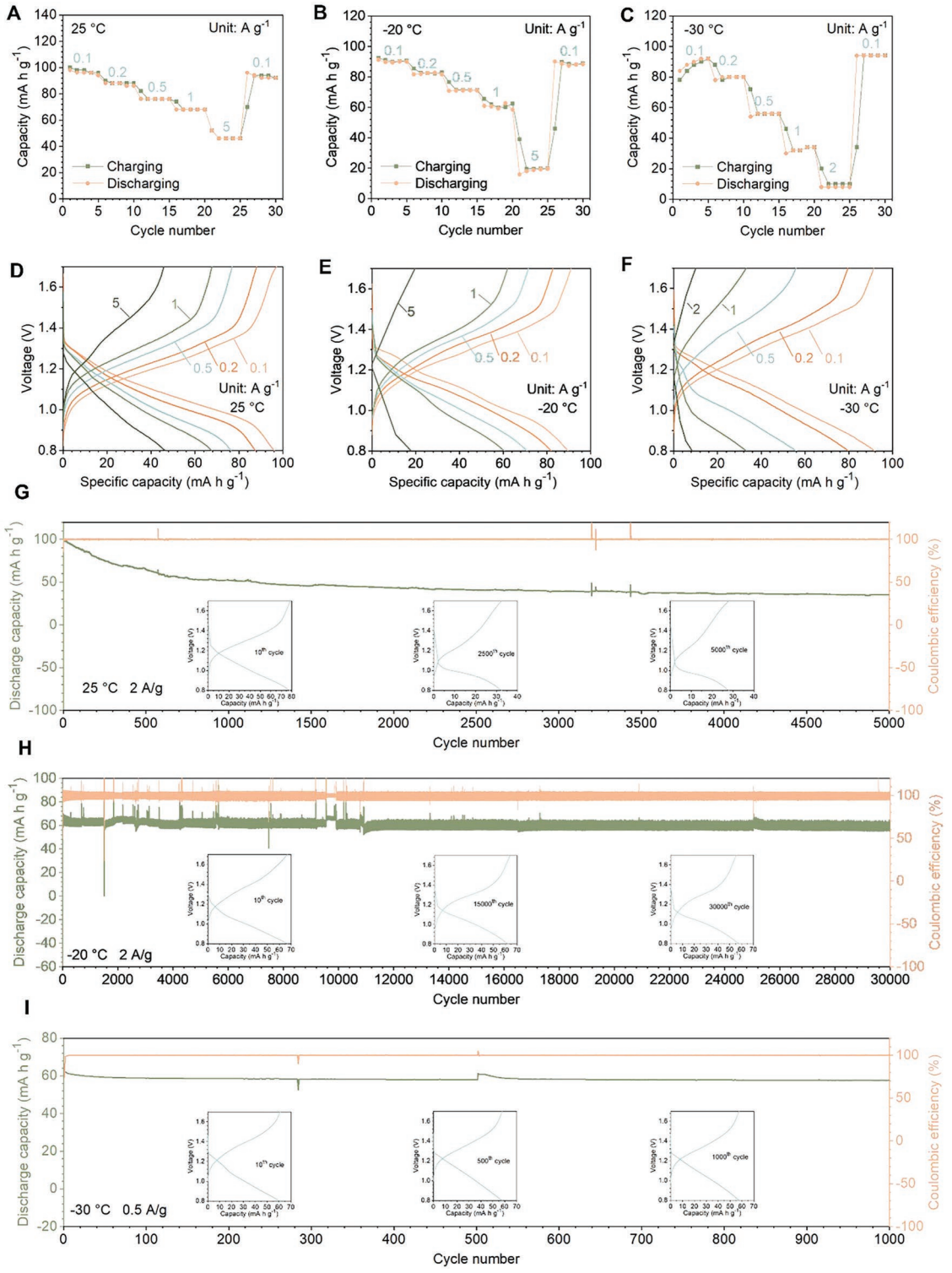

Figure 3. Electrochemical performance of the Zn||PVA-416||PANi batteries at 25 °C, −20 °C, and −30 °C. A–C) Rate performance of the batteries. D–F) Galvanic charge–discharge curves of the batteries. G–I) Cycling performance of the batteries. Insets are the galvanic charge–discharge curves at different cycles.

92, 80, 56, 34, and 8 mA h g^{-1} at current densities of 0.1, 0.2, 0.5, 1, and 2 A g^{-1}, respectively. For all temperatures, the final low-current cycles showed similar capacities as the initial low-current cycles, implying that the decrease in capacity at higher currents can be mainly attributed to the ion transport kinetics rather than the structural degradation of the electrode or the

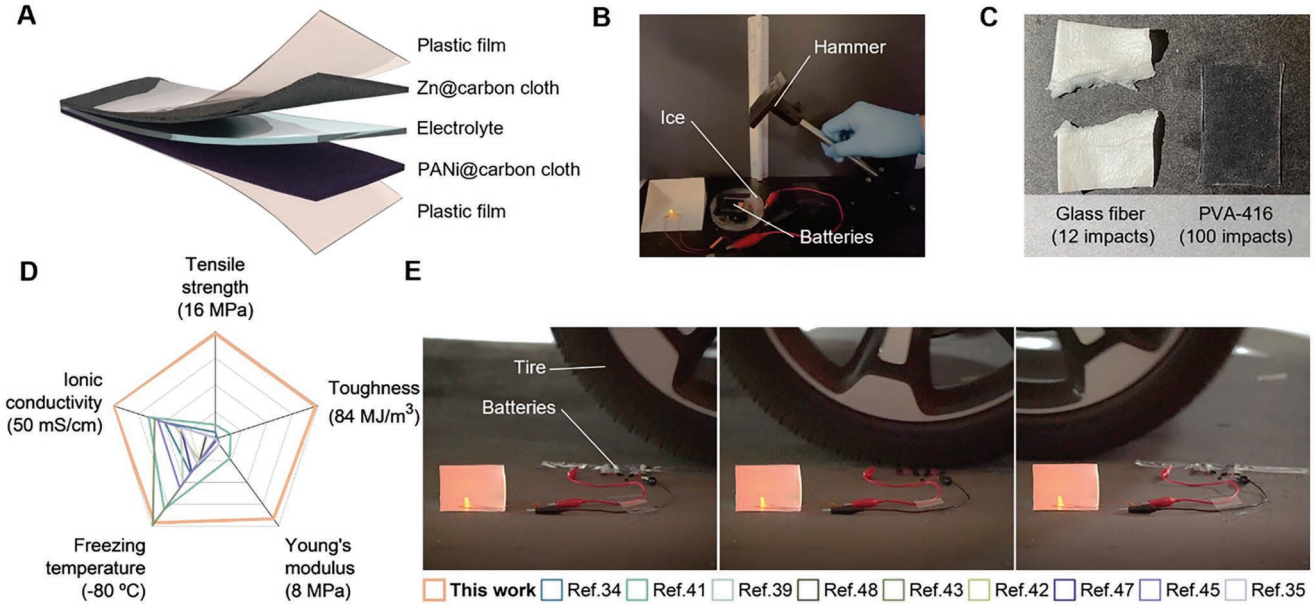

Figure 4. Durable soft-pack batteries enabled by the mechanical and thermal robustness of the hydrogel electrolyte. A) Schematics of the soft-pack battery. B) Hammer test setup. A metal rod (196 g) was used to connect a "hammerhead" (164 g) with a free-rotating axis fixed on the table to construct the "hammer". During the impact events, the "hammerhead" was lifted to 16 cm above the batteries; estimated energy and force per impact event were 1952 J m^{-2} and 130 N, respectively. C) A photograph showing the glass fiber separator and the PVA-416 after impacts. D) Radar plot comparing the properties of the hydrogel electrolyte with the state of the art. For all variables, zero is at the center of the plot. The maxima and increments (represented by the thin grey lines) of different variables are listed here (units as shown in the figure): Tensile strength, 16, 4; Toughness, 84, 21; Young's modulus, 8, 2; Freezing temperature, –80 °C, –20 °C; ionic conductivity (at room temperature), 50, 12.5. E) Snapshots of a car running over the soft-pack batteries.

electrolyte. The voltage window of the charging–discharging plateau (Figure 3D–F) matched that of the redox peaks from the CV. The cycling performances were also evaluated at various temperatures. As shown in Figure 3G–I, at 2 A g^{-1}, the battery provided a reversible capacity of 52.2 and 57.5 mA h g^{-1} after 1000 cycles at 25 °C and 30 000 cycles at –20 °C, respectively, with an imperceptible decrease in capacity at –20 °C, showing its ultrahigh stability. The decrease in capacity at 25 °C (Figure 3G) may be attributed to the deprotonation and swelling/shrinking of PANi,[85–87] which might be alleviated at low temperatures, leading to higher stability. When tested at –30 °C, the battery displayed a reversible capacity of 57.5 mA h g^{-1} after 1000 cycles at 0.5 A g^{-1}, with a small 5% capacity fading compared to the 10th cycle. The batteries could even function at –40 °C and –45 °C, benefitting from the high anti-freezing performance of the hydrogel (Figure S24, Supporting Information). Overall, the battery's high stability and temperature tolerance were enabled by the anti-freezing, dendrite retarding, and reversible zinc chemistry enabling hydrogel electrolyte.

To further demonstrate the dendrite suppression capability and reversible zinc chemistry, the Zn anodes were analyzed after the Zn||PANi batteries were cycled 100 times (48 h), with glass fiber separator/416 solution or PVA-416 as the electrolytes. While both electrolytes achieved dendrite-free (by scanning electron microscopy, Figure S25D,G, Supporting Information) and reversible Zn chemistry (by X-ray powder diffraction, Figure S26, Supporting Information), the zinc deposition was less uniform when the glass fiber separator was used (Figure S25E,F,H,I, Supporting Information), and some zinc deposited into the glass fiber matrix (Figure S25J,K, Supporting Information), which made the batteries prone to shorting. The enhanced uniformity could be a result of the high hydrogel strength,[13–16] which benefits the battery stability.

To demonstrate the impact resistance and anti-freezing capability at the device level, low-temperature hammer tests were conducted on the soft pack batteries (**Figure 4**A; Figure S27, Supporting Information). The PVA-416 battery was able to withstand at least eight times of impacts compared to the one with glass fiber separators (Figure 4B,C; Movies S1 and S2, Supporting Information; estimated energy and force per impact event were 1952 J m^{-2} and 130 N, respectively). More impressively, the soft-pack battery with PVA-416 electrolyte could also withstand being repeatedly run over by a car weighing 1750 kg (Figure 4E; Figure S28 and Movie S3, Supporting Information). Overall, a hydrogel electrolyte that supported stable low-temperature operation for over 30 000 cycles, and with better impact resistivity and zinc deposition uniformity compared to the conventional glass fiber separator, was demonstrated.

2.5. Generality of Method

The co-nonsolvency-"salting-out" method is also applicable to other material combinations to produce strong, anti-freezing, and mass-transport-friendly electrolytes. To demonstrate its generality, the 416 solution as used previously can be combined with different hydrogels, such as open-cell porous poly(*N*-isopropylacrylamide) (PNIPAAm) and poly(*N*-tertbutylacrylamide-*co*-acrylamide) (P(NTBAAm-*co*-AAm)) hydrogels made with co-nonsolvency (Figures S29A,B and S30A,B,

Supporting Information), to increase their temperature tolerance (Figure S29C, Supporting Information) and toughness (Figures S29D and S30C, Supporting Information). The Zn‖PNIPAAm‖PANi battery could cycle at 0.1 A g^{-1} at −20 °C (Figure S29E, 55.4 mA h g^{-1} capacity at the 100th cycle), demonstrating the anti-freezing property of the electrolyte. As another demonstration, the same open-cell porous PVA hydrogel can be combined with another solution (446 solution, in which the mass ratio of $KAc/ZnAc_2 \cdot 2H_2O/H_2O$ is 4/4/6) to make the PVA-446 hydrogel electrolyte. The new electrolyte combined with a revised operation voltage window can achieve a more stable Zn‖PANi battery at 25 °C (Figure S31, Supporting Information), possibly because the lower pH of the 446 solution compared to that of the 416 solution (7.26 and 8.37, respectively) can decrease the deprotonation speed of PANi. The PVA-446 electrolyte is also usable in freezing temperatures (Figure S31E, Supporting Information), which shows the battery operation over 3000 cycles at −20 °C.

3. Conclusion

Flexible aqueous batteries are promising for future soft electrical devices because of their intrinsic safety and cost-effectiveness but are limited by their suboptimal temperature tolerance and impact resistance despite their importance in ensuring stable battery operation. In this work, an approach to achieve a hydrogel electrolyte that has anti-freezing properties, high mechanical robustness, enhanced mass transport, and suppressed dendrites and side reactions was proposed by synergistically utilizing co-nonsolvency and "salting-out" with $KAc/ZnAc_2$ solution. The quasi-solid-state anti-freezing battery made with this hydrogel electrolyte exhibited ultrahigh capacity retention over 30 000 cycles at 2 A g^{-1} at −20 °C and could withstand repeated impacts from a hammer or run-over by a vehicle. Following this strategy, this platform may be expanded with other salts and processes for broader types of battery systems. This work may broaden the application conditions of soft electrical devices and provide one novel approach for next-generation flexible batteries.

4. Experimental Section

Materials: Poly(vinyl alcohol) M_w 31 000–50 000 (363158), M_w 89 000–98 000 (341584), Mowiol 56–98 (10851), potassium acetate (≥99.0%, P1190), zinc acetate dihydrate (383058), ammonium persulfate (ACS reagent, 248614), poly(ethylene glycol) diacrylate (PEGDA, average M_n 700, 455008), aniline (ACS reagent, 242284), *N*-tert-butylacrylamide (NTBAAm, 97%, 411779), *N*,*N*'-methylenebis(acrylamide) (MBAA, 99%, 146072), sodium sulfate (ACS reagent, 239313), boric acid (BioReagent, B6768), zinc sulfate heptahydrate (ACS reagent, 221376), sodium citrate tribasic dihydrate (ACS reagent, S4641), zinc perchlorate hexahydrate (4014239), potassium citrate tribasic monohydrate (99–100.5%, 25107), sodium carbonate (≥99.0%, S7795), sodium acetate (≥99.0%, S8750), and zinc chloride (≥98%, 208086) were purchased from Sigma–Aldrich. Dimethyl Sulfoxide (DMSO) (Certified ACS, D128), hydrochloric acid (Certified ACS Plus, A144), and hexanes (HPLC Grade, H302) were purchased from Fisher chemical. Acrylamide (AAm, 98.5%, 164835000) and *N*-isopropylacrylamide (NIPAAm, 99%, stabilized, 412785000) were purchased from Acros Organics. 2-hydroxy-2-methylpropiophenone (Darocur 1173, >96.0%, H0991) and zinc(II) trifluoromethanesulfonate (>98.0%, T1294) were purchased from TCI. Zinc bis(trifluoromethylsulfonyl)imide was purchased from DoDoChem. Zinc nitrate hexahydrate (min. 98%) was acquired from STREM Chemicals, Inc. Deuterium oxide with DSS was purchased from Cambridge Isotope Laboratories, Inc. Copper foil (9 um), coin cell case (CR2032), spacer (15.8 × 1.5 mm), and funnel spring (15.4 × 1.1 mm) were provided by Canrd. Zinc foil (0.07 mm) was provided by LEISDENT. Commercial glass fiber separators (Whatman GF/C 1822-070) were obtained from Cytiva. ELAT hydrophilic plain carbon cloth (1591002) was purchased from the Fuel Cell Store. Prior to use, the carbon cloth was subjected to 20 min oxygen plasma treatment with a PDC-001 plasma cleaner from Harrick Plasma.

Fabrication of the PVA Hydrogels: To fabricate the open-cell porous PVA hydrogels, PVA solutions with 100% water and 100% DMSO as the solvent were prepared by adding PVA and the solvent into a sealed glass jar to the desired weight percentage (10%, 15%, or 20%), the mixtures were heated to 95 °C in a water bath and stirred at 200 rpm for up to 4 h to yield transparent and homogeneous solutions. Then, the PVA aqueous solution and the PVA DMSO solution were mixed in a centrifuge tube to the desired weight ratio (3:7, 4:6, 5:5, 6:4, 7:3, 8:2) and centrifuged at 3,000 rpm for 90 s to remove the bubbles. Last, the mixture was transferred into glass molds, and the entire assembly was put in a −20 °C freezer overnight to form the hydrogel. Then, the hydrogel was taken out of the mold and was put in a sealed container at room temperature for different durations (0, 1, 3, or 7 days), then was immersed in the 416 solution for 3 days, during which the solution was exchanged for at least five times to ensure the complete substitution of the liquid component in the hydrogels.

It was the best practice to do the mixing, degassing, and transferring as fast as possible to keep the solution hot during these processes because the gelation could be fast (especially for the ones with a 6:4 water to DMSO ratio and high PVA concentrations), and the hydrogel could not be in the desired shape if the gelation happened before the mixture was transferred into the glass mold.

To fabricate the semi-closed-cell PVA, M_w 195k PVA and water were added into a sealed glass jar to the desired weight percentage (15%), and the mixture was heated to 95 °C with a water bath and was stirred at 200 rpm for up to 4 h to yield a transparent and homogeneous solution. Then, the PVA aqueous solution was transferred into a centrifuge tube and then centrifuged at 3000 rpm for 90 s to remove the bubbles. Last, the degassed solution was transferred into a glass mold, and the entire assembly was put in a −20 °C freezer overnight to freeze the solution. The frozen solution was then taken out of the mold and was directly immersed in the 416 solution for 3 days, during which the solution was exchanged at least five times.

The open-cell hydrogel used to compare with the semi-closed-cell hydrogel has the following recipe: M_w 195k PVA, 15 wt%, 6:4 DMSO to water ratio, aged for 7 days and then soaked in the 416 solution.

The recipes used to compare different liquids in the hydrogel: Hydrogels were M_w 195k PVA, 15 wt%, 6:4 DMSO to water ratio, aged for 7 days. Then, they were soaked in water, or the 416 solution, or a zinc sulfate solution (mass ratio of zinc sulfate heptahydrate to water was 0.575 to 1), or a sodium citrate solution (mass ratio of sodium citrate tribasic dihydrate to water was 0.441 to 1) for 3 days. During the soaking, the salt solutions and water were exchanged at least five times.

Fabrication of the PNIPAAm and the P(NTBAAm-co-AAm) Hydrogels: To make the PNIPAAm precursor, the NIPAAm monomers were first purified by dissolving 50 g of NIPAAm in 600 mL hexane at 60 °C. After dissolution, the solution was put in an ice bath, and the monomers (precipitation) were filtered out. Then, 1150 mg of the purified monomers, 95 mg PEGDA, and 5 µL Darocur 1173 were mixed with a 1 mL mixture of $DMSO/H_2O$ (DMSO to H_2O ratio = 4:6 v/v).

To make the P(NTBAAm-*co*-AAm) precursor, 200 mg NTBAAm, 100 mg AAm, 150 mg MBAA, 25 µL of Darocur 1173, 3.5 g DMSO, and 1.5 g H_2O were mixed.

To fabricate the hydrogels, the precursor solutions were injected into glass molds and received 20 s of UV irradiation (Dymax ECE 5000). The resulting PNIPAAm hydrogel was then completely dialyzed in DI

water and freeze-dried (liquid nitrogen for freezing, Labconco FreeZone 1 freeze-dryer for drying); then soaked in DI water to fabricate the PNIPAAm with no salt, or soaked in the 416 solution to fabricate the PNIPAAm with salt. The P(NTBAAm-*co*-AAm) hydrogel from the UV polymerization was then soaked in DI water to fabricate the hydrogel with no salt, or soaked in the 416 solution to fabricate the hydrogel with salt.

Fabrication of the Polyaniline Cathodes: The procedure was adapted from this work.[34] 0.23 g ammonium persulfate (APS) was added to 5 mL 1 M hydrochloric acid solution (HCl) in a beaker. In another beaker, the carbon cloth was immersed in a mixture of 0.36 g aniline and 15 mL 1 M HCl solution. Both beakers were cooled to 4 °C in a fridge. Then, the APS solution was added to the aniline mixture to initiate the reaction. After 1 h, the carbon cloth (with PANi on it) was taken out from the beaker, washed with water and ethanol, and dried at 60 °C for 24 h. The product had a purple color. The mass loadings were ≈0.5 mg cm^{-2}, measured by an electronic scale (ME104E, METTLER TOLEDO, 0.1 mg). To fully utilize the polyaniline deposited on the 3D structure, the cathodes were gently wetted with the 416 solution before use.

Fabrication of the Zn@Carbon Cloth Anodes: The Zn@carbon cloth electrodes were used instead of the zinc foils to assemble the soft-pack batteries to enhance flexibility. The procedure was adapted from this work.[23] The Zn was electrodeposited on a carbon cloth using a Keithley 2450 sourcemeter with a –40 mA cm^{-2} current density for 10 min in a freshly-prepared electrolyte made of 12.5 g zinc sulfate heptahydrate, 12.5 g sodium sulfate, 2 g boric acid, and 100 g water. A carbon cloth of the same size was used as the counter electrode. After the deposition, the product was washed with water and dried in the ambient overnight. The product had a silver color. The mass loadings were ≈10 mg cm^{-2} measured by an electronic scale (ME104E, METTLER TOLEDO, 0.1 mg). To fully utilize the Zn deposited on the 3D structure, the anodes were gently wetted with the 416 solution before use.

Mechanical Characterizations: Tensile, compression, and puncture tests were conducted with a Cellscale Univert. Tensile moduli were obtained by calculating the slope of the stress–strain curves, tensile strengths were determined by the highest point on the stress–strain curves, and toughnesses were calculated by integrating the areas under the stress–strain curves. Error bars represent standard deviations from three to four independent measurements.

For the puncture test, the pin holder and sample holders (outer diameter 4 cm, inner diameter 2 cm) were 3D printed using polylactic acid with a Creality Ender3. A stainless-steel rod (2 mm diameter, from Xingyheng) was used as the penetrating pin. The sample holders were held together with paper clips. During puncture tests, the pin started moving down from the position of the samples' top surface until breakage occurred. The puncture forces were divided by the sample thicknesses and plotted against the displacement distances of the pin.

For low-temperature tensile tests, a temperature probe (Omega HH806AU with type K probe) was attached to the sample clamp. The samples and clamps were placed in a glass cylinder, which was used to hold the dry ice. The samples and clamps were then immersed under dry ice cobbles (Penguin brand) until the temperature readout was below –30 °C, where neither the sample nor the temperature probe was in direct contact with the dry ice. Then, the tensile tests were immediately started. The temperature readouts during the tests were in the range of –25 to –33 °C.

Scanning Electron Microscopy: All hydrogel samples were cut into small pieces (≈5 mm length) and dialyzed in DI water for at least 7 days to completely get rid of the salt ions or DMSO that were in the hydrogel, during which the water was exchanged at least five times. Then, the hydrogels were rapidly immersed in liquid nitrogen (rather than floating on it, to ensure minimal ice templating which could disrupt the original morphology of the hydrogel) until no bubble was coming from the sample. The samples were then broken into smaller pieces by being hit with a steel rod while immersed in liquid nitrogen. The samples were then freeze-dried with a Labconco FreeZone 1 freeze-dryer operating at 0.022 mbar for 48 h. The scanning electron microscopy (SEM) was conducted using a ZEISS Supra 40VP with 9 kV accelerating voltage. The fracture surfaces generated by the steel rod hitting were used to record the SEM images because the pores on the other surfaces might have collapsed during the freezing process.

Nuclear Magnetic Resonance Spectroscopy: The hydrogel sample was prepared by adding 13.8 mg PVA-416 to 0.7 g DSS-containing-D_2O where DSS (sodium 2,2-dimethyl-2-silapentane-5-sulfonate) was used as the internal standard. The control sample was prepared by adding 13.8 mg solution (1 wt% DMSO in water) to 0.7 g DSS-containing-D_2O. The nuclear magnetic resonance (NMR) tests were done using a Bruker AV400 with 32 scans for each sample.

Coin Cell Testing: For all tests, the coin cells were assembled with a TMAXCN hydraulic crimping machine with 1000 psi pressure and were tested with a LANDT CT3002AU battery tester. The –20 °C environment was created using a freezer (Whynter CUF-110B), and the temperature was double-checked with a thermometer (Omega HH806AU with type K probe) whose probe was attached to the coin cell shell. The temperature in the freezer had periodical fluctuation, which could influence the coin cell output. The –30 °C, –40 °C, and –45 °C environments were created using a cooling bath with ethanol (EYELA PSL-1810). The coin cells were put in Ziploc bags and immersed in ethanol, and the temperatures were double-checked with the thermometer.

To compare $KAc/ZnAc_2$ solutions of different concentrations, Zn||Cu half cells were assembled with copper foils, zinc foils, and glass fiber separators, which were cut into 20, 14, and 20 mm diameter disks, respectively. 100 uL of the electrolytes was added to each coin cell during the assembly.

To compare the open-cell and close-cell hydrogels, Zn||Zn symmetric cells were made with zinc foils and hydrogel electrolytes, which were cut into 10 and 20 mm diameter disks, respectively. 0.5 mA cm^{-2}, 0.1 mA h cm^{-2}, and 50 cycles were used to test the cells at –20 °C, and 2 mA cm^{-2}, 0.1 mA h cm^{-2}, 50 cycles were used to test the cells at 25 °C.

To compare the calendar aging performance of the hydrogel and the liquid electrolyte, Zn||Cu half cells were assembled with copper foils, zinc foils, and PVA-416 hydrogels (or glass fiber separators), which were cut into 20, 14, and 20 mm diameter disks, respectively. 100 uL of the 416 solution was added to the glass fiber separator. The activation process was done by depositing Zn on Cu and then stripping immediately (to 0.7 V, with the same current density), which consisted of six cycles: 0.195 mA cm^{-2} for 10 min (three cycles) followed by 0.5 mA cm^{-2} for 30 min (three cycles). The aging performance was tested by first depositing Zn at 0.5 mA cm^{-2} current for 30 min, then resting (open circuit) the cell for 5 h, and stripping Zn using the same current density to 0.7 V. The efficiencies were calculated as

$$\text{Efficiency} = \frac{\text{Stripped capacity (mAh)}}{\text{Deposited capacity (mAh)}} \quad (1)$$

To test the Zn||hydrogel||PANi cells, zinc foils and hydrogel electrolytes were cut into 14 and 20 mm diameter disks, and the carbon cloths with PANi were cut into pieces (1 cm^2 area). For the cycle tests at 25 °C, the coin cell was activated using 0.1, 0.2, 0.5, and 1 A g^{-1} currents (one cycle for each). For the cycle tests at –20 °C and –30 °C, the coin cell was activated using a 0.1 A g^{-1} current for one cycle.

Raman Spectroscopy: The Raman spectra were collected by a Renishaw inVia Raman Microscope equipped with a 633 nm laser. The equipment was calibrated with a silicon standard before use. Data were collected with 10 s exposure time, 50% laser power, and five accumulations. Data were normalized in such a way that the intensity of all samples at 3230 cm^{-1} wavenumbers was the same.

Ionic Conductivity: Ionic conductivities were tested with a CHI660e electrochemical workstation (CH Instruments) using electrochemical impedance spectroscopy mode. Carbon clothes were used as electrodes. The two electrodes were parallelly fixed on the same side of a glass slide with double-sided tapes with 2.128 cm distance in between. A hydrogel membrane with 1.882 cm width and 0.089 cm thickness was put on top of the electrodes, and another piece of glass slide was put on top of the hydrogel membrane. Binder clips were used to clamp the two glass slides, which ensured good contact between the hydrogel and the electrode. The bulk resistances were used to calculate the ionic

conductivity, which could be estimated as the high-frequency intercept of the Nyquist plots with the real axis. Based on the testing geometry, the area in the formula was hydrogel thickness multiplied by width:

$$\text{Ionic conductivity}\left(\text{mS cm}^{-1}\right) = \frac{1000 \times \text{Distance between the electrodes (cm)}}{\text{Bulk resistance}\,(\Omega) \times \text{hydrogel thickness} \times \text{width}\left(\text{cm}^2\right)} \quad (2)$$

The temperature control was done by sealing the setup in Ziploc bags and immersing it in an ethanol cooling bath (EYELA PSL-1810) or putting the setup on top of a hot plate. The temperatures were double-checked with a thermometer (Omega HH806AU with type K probe).

Transference Number: A previously reported method[31,34] was used to test the transference number of the PVA-416 electrolyte. Zn||Zn symmetric coin cells were assembled using a PVA-416 hydrogel electrolyte, and electrochemical impedance spectroscopy and current–time measurements were conducted. The transference number was calculated as

$$t = \frac{R_{\text{cell}}}{R_{\text{DC}}} = \frac{R_{\text{cell}} I_{\text{DC}}}{0.02\ \text{V}} \quad (3)$$

where R_{cell} is resistance before polarization and I_{DC} is the steady state current.

Cyclic Voltammetry: The data were collected with a CHI660e electrochemical workstation (CH Instruments), and the coin cells were connected to the machine via a coin cell clamp.

Differential Scanning Calorimetry: DSC Q2000 Calorimeter (TA Instruments) with an RC-90 cooling system was used to record the DSC data. The samples were initially equilibrated at 15 °C, then cooled to –90 °C at a 2 °C min^{-1} rate. Then, the samples were held at –90 °C for 30 min and heated to 15 °C at a 2 °C min^{-1} rate. Empty pans were used as the reference sample. The sample loadings were ≈25 mg. As liquid has a large tendency to overcool, the melting temperatures measured from the heating process are regarded as the solid–liquid transition temperatures for the liquid samples.

Testing the Freezing Temperature of the PVA-416 Hydrogel: The PVA-416 was put in a Ziploc bag and immersed in the cooled ethanol (EYELA PSL-1810) for 24 h. The temperatures were double-checked with the thermometer (Omega HH806AU with type K probe).

X-ray Powder Diffraction: The zinc anodes were characterized by a PANalytical X'Pert PRO with a Cu Kα radiation source. Prior to the experiment, the zinc anodes were gently washed with DI water, then dried at 50 °C to remove the residual salts on them.

Soft-Pack Batteries: PANi@carbon cloth and Zn@carbon cloth electrodes were used to make the soft-pack batteries. The carbon cloth electrodes were connected to the wires (B-30-1000, VT corporation) with copper tapes (3 M 1181), and the electrode/copper tape/wire assemblies were fixed on the plastic sheets (Scotch self-seal laminating pouches) via the Devcon 5-minute epoxy. The hydrogels (500 µm thick) were then sandwiched between the two electrode/plastic sheet assemblies. The plastic sheets (as the enclosure of the batteries) were cut to the desired sizes and pressed together to seal. Scotch Super 33+ tapes were then used to seal the edges of the plastic sheets. The batteries with glass fiber separators were made with two layers of glass fiber, with a total thickness of 520 µm. The soft-pack batteries were used in the hammer test and the run-over test. In these tests, two batteries were connected in series to provide enough voltage to lit the LED.

Hammer Test: A home-built hammer test setup was employed in pursuit of achieving repeatable impact forces in every impact event. An AP180 mounting plate (Thorlabs) was used as the joint that allows rotation with minimal resistance. The "hammer" consisted of a metal rod and a compatible mounting plate as the "hammerhead". In each of the impact events, the "hammerhead" was lifted to 16 cm above the batteries. The batteries and blocks of ice were equilibrated in a –20 °C freezer before the tests. The tests were done in ambient conditions. During the test, the batteries were put on a block of ice to de-escalate the increase in temperature. Infrared videos were recorded using a TiX580 thermal imager from FLUKE. A high-speed camera (Phantom VEO 710 L) was utilized to record the duration of the impact events at 3000 fps (data not shown). The impact energy and force were calculated from the height (16 cm), the weight of the hammerhead and the rod (164 and 196 g, respectively), contact area (3 cm by 7 mm), rod length (26 cm), and duration of the impact (1/300 s).

The energy was calculated by

$$\frac{\left(0.164\,\text{kg} \times 0.16\,\text{m} + 0.196\,\text{kg} \times \frac{0.16\,\text{m}}{2}\right) \times 9.8\,\text{m s}^{-2}}{0.03\,\text{m} \times 0.007\,\text{m}} = \frac{0.41\,\text{J}}{2.1 \times 10^{-4}\,\text{m}^2} = 1952\left(\text{J m}^{-2}\right) \quad (4)$$

Force was calculated by

$$\text{Force (N)} \times \frac{1}{300}\,\text{s} \times 0.26\,\text{m} = \text{Radial velocity}\left(\text{rad s}^{-1}\right) \times \text{Rotational Inertia}\left(\text{kg m}^2\right) \quad (5)$$

where

$$\text{Rotational Inertia} = \frac{0.196\,\text{kg} \times (0.26\,\text{m})^2}{3} + 0.164\,\text{kg} \times (0.26\,\text{m})^2 = 0.0155\,\text{kg m}^2 \quad (6)$$

and

$$\frac{0.0155\left(\text{kg m}^2\right) \times \left(\text{Radial velocity}\right)^2}{2} = 0.41\,\text{J} \quad (7)$$

Car Run-Over Test: A passenger vehicle with a curb weight of 1750 kg and equipped with 245 mm wide tires was used in the test. The tests were done at ≈17 °C.

Supporting Information

Supporting Information is available from the Wiley Online Library or from the author.

Acknowledgements

Y.Y. and S.D. contributed equally to this work. This research was supported by the NSF CAREER award 1724526. The authors would like to express gratitude to Prof. Steven Nutt, Yunpeng Zhang, and Zehan Yu from the University of Southern California for their kind help with the DSC measurements.

Conflict of Interest

The authors declare no conflict of interest.

Data Availability Statement

The data that support the findings of this study are available from the corresponding author upon reasonable request.

Keywords

anti-freezing, co-nonsolvency, poly(vinyl alcohol), salting-out, tough hydrogels, zinc-ion batteries

Received: December 13, 2022
Revised: January 4, 2023
Published online:

[1] T. R. Ray, J. Choi, A. J. Bandodkar, S. Krishnan, P. Gutruf, L. Tian, R. Ghaffari, J. A. Rogers, *Chem. Rev.* **2019**, *119*, 5461.
[2] S.-H. Sunwoo, K.-H. Ha, S. Lee, N. Lu, D.-H. Kim, *Annu. Rev. Chem. Biomol. Eng.* **2021**, *12*, 359.
[3] P. Rothemund, Y. Kim, R. H. Heisser, X. Zhao, R. F. Shepherd, C. Keplinger, *Nat. Mater.* **2021**, *20*, 1582.
[4] S. I. Rich, R. J. Wood, C. Majidi, *Nat. Electron.* **2018**, *1*, 102.
[5] C. A. Aubin, S. Choudhury, R. Jerch, L. A. Archer, J. H. Pikul, R. F. Shepherd, *Nature* **2019**, *571*, 51.
[6] C. A. Aubin, B. Gorissen, E. Milana, P. R. Buskohl, N. Lazarus, G. A. Slipher, C. Keplinger, J. Bongard, F. Iida, J. A. Lewis, R. F. Shepherd, *Nature* **2022**, *602*, 393.
[7] M. A. Bell, J. C. Weaver, R. J. Wood, *Soft Rob.* **2021**, *9*, 991.
[8] D. Floreano, R. J. Wood, *Nature* **2015**, *521*, 460.
[9] M. Wang, D. Vecchio, C. Wang, A. Emre, X. Xiao, Z. Jiang, P. Bogdan, Y. Huang, N. A. Kotov, *Sci. Rob.* **2020**, *5*, eaba1912.
[10] J.-P. Jones, M. C. Smart, F. C. Krause, W. C. West, E. J. Brandon, *Joule* **2022**, *6*, 923.
[11] V. Viswanathan, A. H. Epstein, Y. M. Chiang, E. Takeuchi, M. Bradley, J. Langford, M. Winter, *Nature* **2022**, *601*, 519.
[12] Z. Liu, D. Wang, Z. Tang, G. Liang, Q. Yang, H. Li, L. Ma, F. Mo, C. Zhi, *Energy Storage Mater.* **2019**, *23*, 636.
[13] K. J. Harry, K. Higa, V. Srinivasan, N. P. Balsara, *J. Electrochem. Soc.* **2016**, *163*, A2216.
[14] R. Zhu, H. Yang, W. Cui, L. Fadillah, T. Huang, Z. Xiong, C. Tang, D. Kowalski, S. Kitano, C. Zhu, D. R. King, T. Kurokawa, Y. Aoki, H. Habazaki, *J. Mater. Chem. A* **2022**, *10*, 3122.
[15] C. Monroe, J. Newman, *J. Electrochem. Soc.* **2005**, *152*, A396.
[16] X. Zhang, A. Wang, X. Liu, J. Luo, *Acc. Chem. Res.* **2019**, *52*, 3223.
[17] L. Chen, Q. An, L. Mai, *Adv. Mater. Interfaces* **2019**, *6*, 1900387.
[18] S. Zhao, Y. Zuo, T. Liu, S. Zhai, Y. Dai, Z. Guo, Y. Wang, Q. He, L. Xia, C. Zhi, J. Bae, K. Wang, M. Ni, *Adv. Energy Mater.* **2021**, *11*, 2101749.
[19] N. Zhang, X. Chen, M. Yu, Z. Niu, F. Cheng, J. Chen, *Chem. Soc. Rev.* **2020**, *49*, 4203.
[20] H. Zhang, X. Liu, H. Li, I. Hasa, S. Passerini, *Angew. Chem., Int. Ed.* **2021**, *60*, 598.
[21] Q. Nian, T. Sun, S. Liu, H. Du, X. Ren, Z. Tao, *Chem. Eng. J.* **2021**, *423*, 130253.
[22] L. E. Blanc, D. Kundu, L. F. Nazar, *Joule* **2020**, *4*, 771.
[23] Y. Zeng, X. Zhang, Y. Meng, M. Yu, J. Yi, Y. Wu, X. Lu, Y. Tong, *Adv. Mater.* **2017**, *29*, 1700274.
[24] M. Yao, Z. Yuan, S. Li, T. He, R. Wang, M. Yuan, Z. Niu, *Adv. Mater.* **2021**, *33*, 2008140.
[25] L. Ma, S. Chen, N. Li, Z. Liu, Z. Tang, J. A. Zapien, S. Chen, J. Fan, C. Zhi, *Adv. Mater.* **2020**, *32*, 1908121.
[26] F. Mo, Z. Chen, G. Liang, D. Wang, Y. Zhao, H. Li, B. Dong, C. Zhi, *Adv. Energy Mater.* **2020**, *10*, 2000035.
[27] Y. Hao, D. Feng, L. Hou, T. Li, Y. Jiao, P. Wu, *Adv. Sci.* **2022**, *9*, 2104832.
[28] J. Cong, X. Shen, Z. Wen, X. Wang, L. Peng, J. Zeng, J. Zhao, *Energy Storage Mater.* **2021**, *35*, 586.
[29] Y. Tang, C. Liu, H. Zhu, X. Xie, J. Gao, C. Deng, M. Han, S. Liang, J. Zhou, *Energy Storage Mater.* **2020**, *27*, 109.
[30] X. Zhang, Z. Pei, C. Wang, Z. Yuan, L. Wei, Y. Pan, A. Mahmood, Q. Shao, Y. Chen, *Small* **2019**, *15*, 1903817.
[31] K. Leng, G. Li, J. Guo, X. Zhang, A. Wang, X. Liu, J. Luo, *Adv. Funct. Mater.* **2020**, *30*, 2001317.
[32] B. Yao, S. Wu, R. Wang, Y. Yan, A. Cardenas, D. Wu, Y. Alsaid, W. Wu, X. Zhu, X. He, *Adv. Funct. Mater.* **2022**, *32*, 2109506.
[33] X. Xiao, X. Xiao, Y. Zhou, X. Zhao, G. Chen, Z. Liu, Z. Wang, C. Lu, M. Hu, A. Nashalian, S. Shen, K. Xie, W. Yang, Y. Gong, W. Ding, P. Servati, C. Han, S. X. Dou, W. Li, J. Chen, *Sci. Adv.* **2021**, *7*, eabl3742.
[34] S. Huang, L. Hou, T. Li, Y. Jiao, P. Wu, *Adv. Mater.* **2022**, *34*, 2110140.
[35] F. Mo, G. Liang, D. Wang, Z. Tang, H. Li, C. Zhi, *EcoMat* **2019**, *1*, e12008.
[36] Y. Zhang, H. Qin, M. Alfred, H. Ke, Y. Cai, Q. Wang, F. Huang, B. Liu, P. Lv, Q. Wei, *Energy Storage Mater.* **2021**, *42*, 88.
[37] J. Wang, Y. Huang, B. Liu, Z. Li, J. Zhang, G. Yang, P. Hiralal, S. Jin, H. Zhou, *Energy Storage Mater.* **2021**, *41*, 599.
[38] Y. Wang, Y. Chen, *Electrochim. Acta* **2021**, *395*, 139178.
[39] Y. Liu, X. Zhou, Y. Bai, R. Liu, X. Li, H. Xiao, Y. Wang, X. Wang, Y. Ma, G. Yuan, *Chem. Eng. J.* **2021**, *417*, 127955.
[40] Z. Pei, Z. Yuan, C. Wang, S. Zhao, J. Fei, L. Wei, J. Chen, C. Wang, R. Qi, Z. Liu, Y. Chen, *Angew. Chem., Int. Ed.* **2020**, *59*, 4793.
[41] M. Chen, J. Chen, W. Zhou, X. Han, Y. Yao, C. P. Wong, *Adv. Mater.* **2021**, *33*, 2007559.
[42] Y. Quan, M. Chen, W. Zhou, Q. Tian, J. Chen, *Front. Chem.* **2020**, *8*, 603.
[43] M. Chen, W. Zhou, A. Wang, A. Huang, J. Chen, J. Xu, C. P. Wong, *J. Mater. Chem. A* **2020**, *8*, 6828.
[44] Y. Chen, J. Zhao, Y. Wang, *ACS Appl. Energy Mater.* **2020**, *3*, 9058.
[45] M. Zhu, X. Wang, H. Tang, J. Wang, Q. Hao, L. Liu, Y. Li, K. Zhang, O. G. Schmidt, *Adv. Funct. Mater.* **2020**, *30*, 1907218.
[46] N. Sun, F. Lu, Y. Yu, L. Su, X. Gao, L. Zheng, *ACS Appl. Mater. Interfaces* **2020**, *12*, 11778.
[47] F. Mo, G. Liang, Q. Meng, Z. Liu, H. Li, J. Fan, C. Zhi, *Energy Environ. Sci.* **2019**, *12*, 706.
[48] R. Chen, X. Xu, S. Peng, J. Chen, D. Yu, C. Xiao, Y. Li, Y. Chen, X. Hu, M. Liu, H. Yang, I. Wyman, X. Wu, *ACS Sustainable Chem. Eng.* **2020**, *8*, 11501.
[49] H. Wang, J. Liu, J. Wang, M. Hu, Y. Feng, P. Wang, Y. Wang, N. Nie, J. Zhang, H. Chen, Q. Yuan, J. Wu, Y. Huang, *ACS Appl. Mater. Interfaces* **2019**, *11*, 49.
[50] T. Wei, Y. Ren, Z. Li, X. Zhang, D. Ji, L. Hu, *Chem. Eng. J.* **2022**, *434*, 134646.
[51] P. M. Xavier, R. I. Widusha, K. Tian, R. Bai, Z. Suo, J. V. Joost, *Adv. Mater.* **2018**, *30*, 1801246.
[52] D. Bao, Z. Wen, J. Shi, L. Xie, H. Jiang, J. Jiang, Y. Yang, W. Liao, X. Sun, *J. Mater. Chem. A* **2020**, *8*, 13787.
[53] S. Wu, M. Hua, Y. Alsaid, Y. Du, Y. Ma, Y. Zhao, C. Y. Lo, C. Wang, D. Wu, B. Yao, J. Strzalka, H. Zhou, X. Zhu, X. He, *Adv. Mater.* **2021**, *33*, 2007829.
[54] J. Cannarella, X. Liu, C. Z. Leng, P. D. Sinko, G. Y. Gor, C. B. Arnold, *J. Electrochem. Soc.* **2014**, *161*, F3117.
[55] R. S. Baldwin, W. R. Bennett, E. K. Wong, M. R. Lewton, M. K. Harris, *Nasa/Tm* **2010**, *1*, 0021170.
[56] S. M. Lanasa, I. T. Hoffecker, S. J. Bryant, *J. Biomed. Mater. Res., Part B* **2011**, *96*, 294.
[57] J. Kovacik, *J. Mater. Sci. Lett.* **1999**, *18*, 1007.
[58] S. Liu, R. Zhang, J. Mao, Y. Zhao, Q. Cai, Z. Guo, *Sci. Adv.* **2022**, *8*, abn5097.
[59] M. Hua, S. Wu, Y. Ma, Y. Zhao, Z. Chen, I. Frenkel, J. Strzalka, H. Zhou, X. Zhu, X. He, *Nature* **2021**, *590*, 594.
[60] S. Duan, S. Wu, M. Hua, D. Wu, Y. Yan, X. Zhu, X. He, *iScience* **2021**, *24*, 102989.
[61] S. Wu, Y. Alsaid, B. Yao, Y. Yan, Y. Zhao, M. Hua, D. Wu, X. Zhu, X. He, *EcoMat* **2021**, *3*, e12085.
[62] R. Khodambashi, Y. Alsaid, R. Rico, H. Marvi, M. M. Peet, R. E. Fisher, S. Berman, X. He, D. M. Aukes, *Adv. Mater.* **2021**, *33*, 2005906.
[63] H. Dong, J. Li, J. Guo, F. Lai, F. Zhao, Y. Jiao, D. J. L. Brett, T. Liu, G. He, I. P. Parkin, *Adv. Mater.* **2021**, *33*, 2007548.
[64] C. Lin, X. Yang, P. Xiong, H. Lin, L. He, Q. Yao, M. Wei, Q. Qian, Q. Chen, L. Zeng, *Adv. Sci.* **2022**, *9*, 2201433.
[65] Y. H. Zhang, C. K. Chan, *J. Phys. Chem. A* **2003**, *107*, 5956.
[66] S. Chen, R. Lan, J. Humphreys, S. Tao, *Energy Storage Mater.* **2020**, *28*, 205.

[67] J. Han, A. Mariani, A. Varzi, S. Passerini, *J. Power Sources* **2021**, *485*, 229329.
[68] Y. Alsaid, S. Wu, D. Wu, Y. Du, L. Shi, R. Khodambashi, R. Rico, M. Hua, Y. Yan, Y. Zhao, D. Aukes, X. He, *Adv. Mater.* **2021**, *33*, 2008235.
[69] Y. Zhao, C. Y. Lo, L. Ruan, C. H. Pi, C. Kim, Y. Alsaid, I. Frenkel, R. Rico, T. C. Tsao, X. He, *Sci. Rob.* **2021**, *6*, eabd5483.
[70] H. Yamauchi, Y. Maeda, *J. Phys. Chem. B* **2007**, *111*, 12964.
[71] D. Mukherji, C. M. Marques, K. Kremer, *Nat. Commun.* **2014**, *5*, 4882.
[72] H. Kojima, F. Tanaka, C. Scherzinger, W. Richtering, *J. Polym. Sci., Part B: Polym. Phys.* **2013**, *51*, 1100.
[73] S. Bharadwaj, N. F. A. Van Der Vegt, *Macromolecules* **2019**, *52*, 4131.
[74] G. J. Lake, A. G. Thomas, *Proc. R. Soc. Lond., Ser. A* **1967**, *300*, 108.
[75] J. Kim, G. Zhang, M. Shi, Z. Suo, *Science* **2021**, *374*, 212.
[76] Z. Wang, C. Xiang, X. Yao, P. L. Floch, J. Mendez, Z. Suo, *Proc. Natl. Acad. Sci. USA* **2019**, *116*, 5967.
[77] S. H. Hyon, W. I. Cha, Y. Ikada, *Polym. Bull.* **1989**, *22*, 119.
[78] H. Hoshino, S. Okada, H. Urakawa, K. Kajiwara, *Polym. Bull.* **1996**, *37*, 237.
[79] T. Tanigami, K. Murase, K. Yamaura, S. Matsuzawa, *Polymer* **1994**, *35*, 2573.
[80] R. Khurana, J. L. Schaefer, L. A. Archer, G. W. Coates, *J. Am. Chem. Soc.* **2014**, *136*, 7395.
[81] M. Charlton, T. D. Hatchard, M. N. Obrovac, *J. Electrochem. Soc.* **2020**, *167*, 080501.
[82] J. Xie, Q. Zhang, *Small* **2019**, *15*, 1805061.
[83] H. Y. Shi, Y. J. Ye, K. Liu, Y. Song, X. Sun, *Angew. Chem., Int. Ed.* **2018**, *57*, 16359.
[84] F. Wan, L. Zhang, X. Wang, S. Bi, Z. Niu, J. Chen, *Adv. Funct. Mater.* **2018**, *28*, 1804975.
[85] Y. Liu, Z. Dai, W. Zhang, Y. Jiang, J. Peng, D. Wu, B. Chen, W. Wei, X. Chen, Z. Liu, Z. Wang, F. Han, D. Ding, L. Wang, L. Li, Y. Yang, Y. Huang, *ACS Nano* **2021**, *15*, 9065.
[86] J. Gong, H. Li, K. Zhang, Z. Zhang, J. Cao, Z. Shao, C. Tang, S. Fu, Q. Wang, X. Wu, *Nanomaterials* **2022**, *12*, 1438.
[87] H.-Y. Shi, Y.-J. Ye, K. Liu, Y. Song, X. Sun, *Angew. Chem.* **2018**, *130*, 16597.